Static and dynamic aspects of spin tunnelling in crystalline magnetic tunnel junctions

2006 J. Phys.: Condens. Matter 18 941

(http://iopscience.iop.org/0953-8984/18/3/012)

INSTITUTE OF PHYSICS PUBLISHING JOURNAL OF PHYSICS: CONDENSED MATTER

J. Phys.: Condens. Matter **18** (2006) 941–956 doi:10.1088/0953-8984/18/3/012

Static and dynamic aspects of spin tunnelling in crystalline magnetic tunnel junctions

C Tiusan[1], M Sicot[1], J Faure-Vincent[2], M Hehn[1], C Bellouard[1], F Montaigne[1], S Andrieu[1] and A Schuhl[1]

[1] Laboratoire de Physique des Matériaux, UMR CNRS 7556, BP 239, 54506 Vandœuvre lès Nancy Cedex, France
[2] Laboratoire SPINTEC, URA 2512, Avenue des Martyrs 38054, Granoble, France

Received 13 October 2005
Published 6 January 2006
Online at stacks.iop.org/JPhysCM/18/941

Abstract

Single-crystal magnetic tunnel junctions employing bcc (100) Fe electrodes and MgO(100) insulating barrier are elaborated by molecular beam epitaxy. The magneto-transport properties are investigated in two extreme regimes. First, for extremely small MgO thickness, we show that the equilibrium tunnel transport in Fe/MgO/Fe systems leads to antiferromagnetic interactions, mediated by the tunnelling of the minority spin interfacial resonance state. Second, for large MgO barrier thickness, the tunnel transport validates specific spin filtering effects in terms of symmetry of the electronic Bloch function and symmetry-dependent wavefunction attenuation in the single-crystal barrier. Within this framework, we present giant tunnel magnetoresistive effects at room temperature (125–160%). Moreover, we illustrate that the interfacial chemical and electronic structure plays a crucial role in the spin filtering. We point out imperfect filtering effects and a strong implication of the minority surface state of Fe on the low voltage variation of tunnel magnetoresistance. The insertion of carbon impurities at the Fe/MgO interface changes radically the voltage response of the tunnel magnetoresistance and activates a resonant tunnelling mechanism via the interfacial resonance state.

1. Introduction

The discovery in 1995 of a tunnel magneto-resistance (TMR) effect at room temperature in amorphous oxide barrier based magnetic tunnel junctions (MTJs) [1] paved the way to intense developments in this field area with many possible application prospects [2]. This subject gained a new dimension with the measure at room temperature of TMR effects in single-crystalline tunnel junctions up to three times larger than in standard amorphous alumina barriers. The large TMR values at RT are extremely important for the potential applications of MTJs in sensors and data storage devices. In the epitaxial Fe(100)/MgO/Fe MTJ, after the pioneering results reported in 2001 by Bowen *et al* [3] (27%-RT), the TMR

ratio has been successfully improved: 67%-RT reported in 2003 by our group [4], 88%-RT reported in 2004 by Yuasa *et al* [5]. Recently, values above 200% have been measured in MgO crystalline oxide based tunnel barriers [6–8]. In our group, we have investigated a large class of MTJ systems employing MgO(100) insulating barriers and different bcc (100) electrodes such as Fe, Co, CoFe, Pd/Fe and their combinations [9]. In these systems we measure giant TMR ratios between 100 and 170%. In this paper we point out the crucial role of the interfacial electronic/chemical structure in the tunnel transport characteristics in Fe(100)/MgO/Fe epitaxial MTJs.

As explained theoretically [10, 11], the large TMR ratios in single-crystal tunnel junctions are determined by the different tunnelling mechanisms and symmetry-related decay rates of the Bloch waves for the majority and the minority spin channels. Roughly, an emitter single-crystalline ferromagnetic (FM) electrode filters the electrons in terms of symmetry; they are subsequently injected across the insulating (I) barrier. The filtering effect can be easily understood from figure 1 where we illustrate the bulk band structure of bcc Fe, along the high symmetry Γ–H direction, for the majority and minority spins. The direction $\Delta = \Gamma$–H corresponds to electrons with $k_{\parallel} = 0$, which propagate along the (100) direction in the crystal. At the Fermi level for the majority electrons we have the following states: a Δ_1 (spd-like character state), a Δ_5 (pd) and a Δ_2' (d). Due to the exchange splitting, at E_F, there is no Δ_1 state for the minority spin. Therefore, one can immediately see that the Fe behaves as a half-metal in terms of the Δ_1 symmetry. Then, the tunnel transport probes: (i) the differences in spin injection (extraction) efficiency (directly related to the interfacial FM/I matching/coupling), and (ii) the differences in decay rates when tunnelling across the barrier. The epitaxial growth of the MgO on Fe, via a rotation by 45° of the MgO lattice with respect to the Fe one, provides the symmetry conservation across the junction stack. One can demonstrate that the Δ_1 state has the smallest decay rate across the MgO, followed by the Δ_5 then the $\Delta_{2,(2')}$.

Consequently [10, 11], for large MgO thickness, in the asymptotic regime, in the parallel (P) configuration, the tunnelling is found to be governed by the Δ_1 state. The conductance in the antiparallel (AP) configuration is very low, being only related to the $\Delta_{5,(2')}$ state propagation, with a larger decay rate. In the AP configuration, an injected Δ_1 state cannot find equivalent symmetry in the opposite electrode with reversed magnetization. The spin asymmetry is predicted to increase above 1000%. On the contrary, when the thickness of the insulating layer decreases, the contribution of the double degenerate pd character state Δ_5 and even $\Delta_{2,(2')}$ becomes significant, the conductivity in the AP state increases and therefore the TMR ratio decreases.

The above simplified picture for tunnelling summarizes the main result of the theoretical predictions [10, 11] considering only the simplified situation where we only consider the electrons having $k_{\parallel} = 0$. This is essentially valid for large insulating thickness (asymptotic regime). The situation gets more complex at low MgO thickness, where the contribution of $k_{\parallel} \neq 0$ electrons becomes significant. Moreover, in the small MgO barrier thickness regime, the tunnel transmission gets strongly affected by resonant effects at the interfaces [10, 11, 13, 14]. Indeed, for the Fe(001)/MgO interface, an interfacial minority state is found above the Fermi energy. Such interfacial resonances, from both sides of the barrier, may couple to each other, leading to a resonant tunnelling mechanism [13], which manifests itself as spikes in the conductance distribution in particular $k_{\parallel}$ points in the two-dimensional Brillouin zone. The width of these spikes is determined by the strength of the coupling in the barrier, which decreases exponentially with the barrier thickness. Consequently, the conductance from an interfacial resonance state is particularly important for extremely thin barriers. Here, the contribution of the resonant assisted tunnelling is major even in the equilibrium regime, and determines the antiferromagnetic coupling interactions observed in our Fe/MgO/Fe

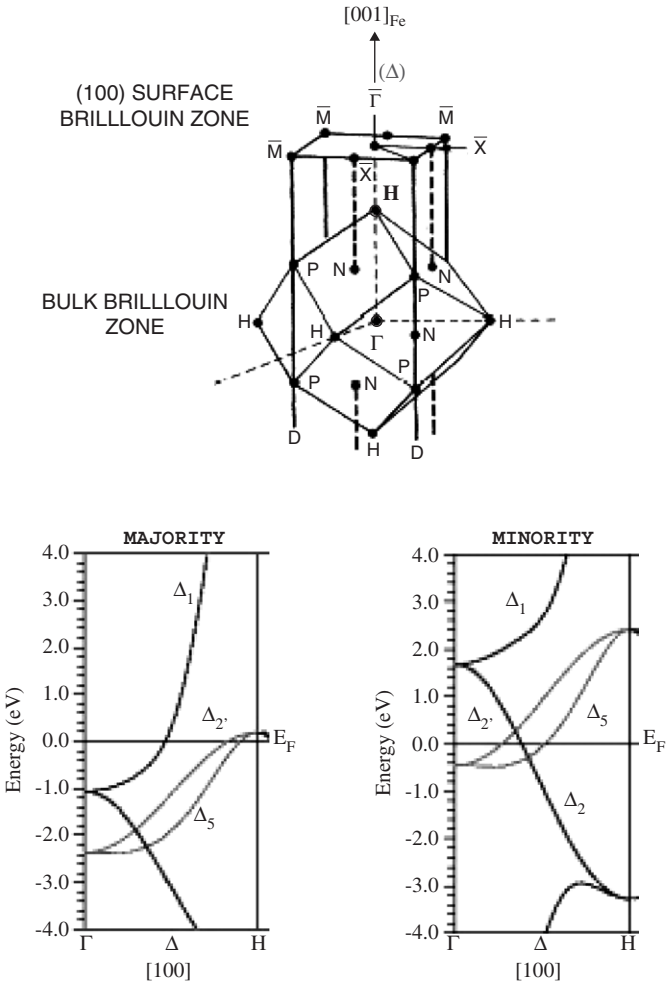

Figure 1. Top: representation of the bulk and the (001) surface Brillouin zone for the bcc Fe. Bottom: Bulk energy bands for the majority and minority spins in bcc Fe.

system [16]. Alternatively, the contribution to the tunnelling of an interfacial state may be activated, by biasing the junction at finite bias voltage, even in the large MgO thickness regime.

2. Sample elaboration

The MTJ multilayer stacks subjected to our studies have been elaborated by molecular beam epitaxy (MBE), in a chamber with a base pressure of 5×10^{-11} Torr. Two sets of samples have been grown on (100) MgO substrates, previously annealed at 600 °C for 20 min. For sample type A, a 50 nm thick bottom Fe layer was deposited at room temperature directly on the MgO substrate. For sample type B, a 10 nm thick seed MgO underlayer was grown at 450 °C on the substrate, before the deposition of the 50 nm thick Fe layer. This MgO under-layer acts as an anti-diffusion barrier which traps the residual carbon impurities and prevents their diffusion within the layers during subsequent annealing stages. Indeed, to improve its surface quality, the bottom Fe layer was annealed at 450 °C for 20 min. The surface RMS roughness after

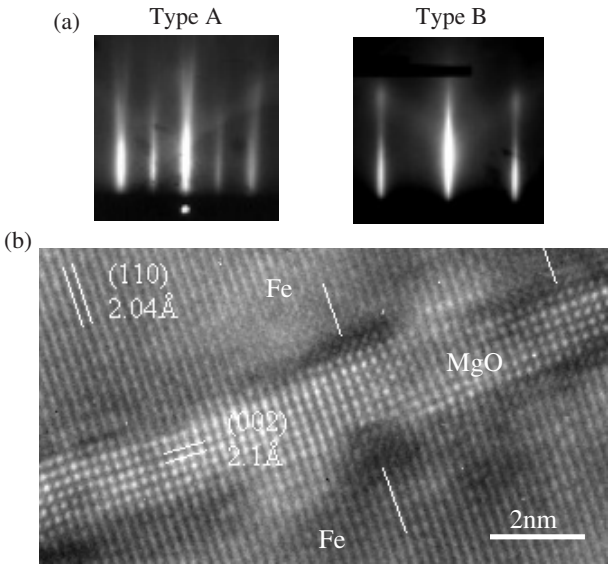

Figure 2. (a) RHEED pattern measured along the [100] direction of the Fe bottom layer in sample type A (left)and sample type B (right). The analysis for sample A highlights additional peaks characteristic of the 2×2 reconstruction. (b) Cross section transmission electron microscopy image of an Fe(100)/MgO/Fe stack.

annealing, estimated from atomic force microscope analysis, was about 0.3 nm. However, the Fe top surfaces post-annealing are not equivalent for samples of types A and B, as highlighted in figure 2(a) containing reflecting high energy electron diffraction (RHEED) patterns. For both sets of samples the RHEED patterns along the [110] direction (not shown here) are identical and they are characteristic of the cubic bcc Fe structure. However, along the [100] direction, the RHEED analysis of sample type A emphasizes a 2×2 reconstruction-related additional pattern, not present for sample B. A complete RHEED analysis concludes that in sample type A the Fe surface post-annealing presents a $c(2 \times 2)$ super-structure. In agreement with results of previous Auger electron spectroscopy and quantitative low energy electron diffraction (LEED) studies [18], we associate this reconstruction with the segregation of C at the Fe(001) surface. Using Auger analysis we checked the chemical nature of the surface and we confirmed that for the sample of type A a carbon layer was segregated during the Fe annealing. Where does the C come from? We observed that the annealing stage of the MgO substrate at 600 °C does not desorb all the C atoms from the surface. When the anti-diffusion 10 nm MgO thick underlayer is not inserted (sample of type A), the residual C atoms diffuse and segregate to the Fe top surface and provide the surface reconstruction during the bottom Fe layer annealing. On the other hand, in sample type B, the trapping under-layer of MgO provides a C free Fe top surface, post-annealing. As will be shown in the following, the chemical structure of the Fe surface has a strong impact on the magneto-transport characteristics of the junctions, mainly reflected by the TMR versus applied voltage behaviour.

On the top of the bottom Fe layer, the MgO insulating layer was epitaxially grown by means of an electron gun. A two-dimensional layer-by-layer growth was observed up to 5 monolayers by means of RHEED intensity oscillations [4, 19]. These oscillations have been used to control precisely the thickness of the barrier in the extremely small thickness range from 3 to 6 monolayers, used for magnetic coupling studies. For the systems used to study the

magneto-transport properties, the thickness of the insulating barrier was fixed to 3.0 nm. This thickness corresponds to the asymptotic regime, where we expect, as predicted theoretically, large magnetoresistive effects. A second magnetic 10 nm thick Fe layer was epitaxially grown on the top of the insulating MgO barrier at 100 °C. It was subsequently annealed for flattening at 380 °C for 10 min for samples of type B whereas for samples of type A this annealing stage was not performed in order to avoid possible structural modification of the bottom Fe-C/MgO interface. This top Fe layer is magnetically hardened by a 20 nm Co over-layer. The stack was capped with a Pd(10 nm)/Au(10 nm) protecting bilayer.

The structural quality of the tunnel junction stack is illustrated by the cross-section transmission electron microscopy picture, depicted in figure 2(b). One can see the epitaxial growth of MgO on Fe. This is a key parameter for the conservation of symmetry from the Fe electrode through the MgO barrier (conservation of $k_{\parallel}$) and has a huge impact on the Bloch wave propagation in the stack. However, dislocations located either at the bottom or at the top Fe/MgO interface (indicated in the picture by dark zones marked by white lines) induce violation of symmetry conservation and therefore have detrimental effects on the symmetry filtering.

After the MBE growth of the multilayer stack, the MTJ structures are patterned by UV lithography and Ar ion etching, step-by-step controlled *in situ* by Auger spectroscopy [4, 19].

3. Spin polarized tunnel transport in Fe/MgO/Fe junctions

3.1. Equilibrium tunnel transport—coupling regime

In the very small MgO thickness regime (three to five monolayers), we observe antiferromagnetic (AF) coupling interactions at room temperature between the two ferromagnetic (F) Fe layers separated by the thin insulating tunnel barrier. We associate these interactions with the transport of spin information across the insulating spacer by equilibrium quantum tunnelling of spin polarized electrons [16]. Equilibrium tunnelling implicates tunnelling of majority and minority electrons from one side to the other of the junction. In the absence of any net bias, the total current across the insulating MgO barrier is zero.

The magnetic properties have been investigated from magnetization versus field loops, performed on continuous multilayer films with lateral sizes above a few millimetres, in order to avoid spurious antiferromagnetic dipolar coupling, introduced by patterning of small size devices. This analysis has been already presented in detail in our previous paper concerning the interlayer coupling by spin polarized tunnelling [16]. We only report here the main results. The interlayer magnetic coupling strength J is extracted from the shift of the minor hysteresis loops (figure 3(a)), taken for the soft magnetic layer in a field window where the hard layer is magnetically 'locked' by an initial magnetization saturation. In figure 3(b), we illustrate the variation of J with the thickness t_{MgO} of the insulating barrier. The AF coupling interactions have been observed for both types of samples, A and B, with and without carbon at the Fe/MgO interface.

In a first step, the experimental points can be adjusted by the continuous line (figure 3), which represents the theoretical coupling strength computed in the simplified free-electron-like framework of Slonczewski [15], as explained in detail in our previous paper [16]. The theoretical curve implicates effective parameters for the electronic transport, specific to the ferromagnetic Fe electrodes and the MgO insulator. However, the model of Slonczewski does not take into account the specific aspects of the spin polarized tunnelling in epitaxial systems, i.e. the equilibrium propagation of different symmetry states for each spin channel, in each

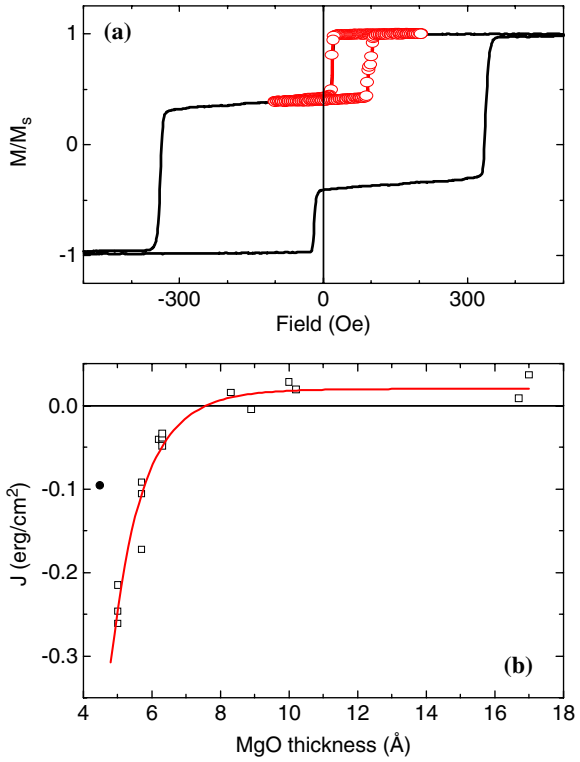

Figure 3. (a) Magnetization versus field curve, respectively minor loop (-o-). From the positive shift of the minor loop H_{ex} one can extract the coupling strength J: $H_{ex} = J/(t_{Fe}M_s)$, where t_{Fe} is the thickness of the Fe bottom layer and M_s the saturation magnetization of Fe. (b) Variation of the coupling strength with the MgO thickness. The open square points represent experimental values and the continuous line a theoretical calculation within the Slonczewski model of coupling by spin-polarized tunnelling.

configuration of magnetizations: (i) in the parallel (P) configuration the $\Delta_{1,5,2'}$ states for the majority spin and $\Delta_{5,2,2'}$ states for the minority; (ii) in the anti-parallel configuration the $\Delta_{5,2'}$ state for the majority and for the minority spin.

On the other hand, Tsymbal *et al* [17] pointed out theoretically the implication of a resonance assisted tunnelling mechanism in the AF coupling by spin polarized tunnelling. In their model, they have shown that an additional resonant tunnelling mechanism should exist in order to explain the sign of the coupling observed in our Fe/MgO/Fe junctions. If we neglect any impurity-associated resonant levels, the interfacial minority resonance of Fe provides the resonant equilibrium tunnelling mechanism, as also shown in the *ab initio* calculations of Dederichs *et al* [13]. Therefore, one can assume that the equilibrium tunnel transport in the AP configuration is dominated by the propagation of the interfacial resonance, related to the surface state of Fe(001). This surface state has been measured by scanning tunnelling microscopy (STM) spectroscopy on Fe(100) surfaces by Stroscio *et al* [12]. It has a d_{z^2} orbital character belonging to the Δ_1 symmetry and is located in the minority spin channel. Recently, scanning tunnelling spectroscopy experiments have validated the presence of the minority surface state for the Fe(001) surface in our samples. This means that the roughness level in our samples is small enough to prevent destruction of the interfacial resonance. Moreover, this surface state seems to be quite solid with respect to low-level disorder (it is not destroyed by terrace

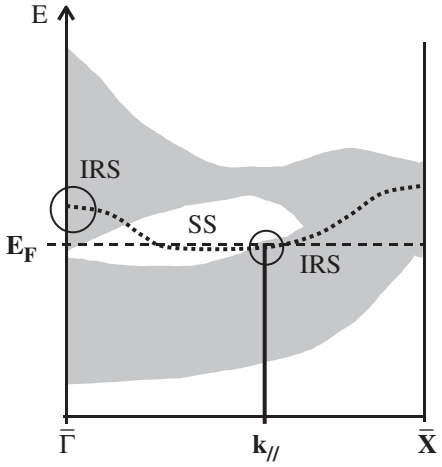

Figure 4. Simplified diagram for the dispersion of the surface energy bands for minority spin in Fe(001) as reported by Stroscio *et al* [12]. The grey zones represent schematic bulk bands, whereas the dashed line the dispersion of the surface state (SS). When the surface state lies within a bulk band, it becomes an interfacial resonance state (IRS), and can contribute to the transport towards the bulk, i.e. in $\bar{\Gamma}$ above E_F and for a certain value $k_{\|} \neq 0$ at E_F.

boundaries, carbon and oxygen contamination). One can imagine that some low-level disorder may even help for coupling of the surface state with the bulk bands, enhancing its contribution to the transport.

Theoretical calculations [10, 11] have shown that the interfacial resonance of Fe is preserved at the Fe(100)/MgO interface. Therefore, in a second step, we could assume that the resonant propagation of the interfacial resonance could be the main origin for the AF coupling observed in our Fe/MgO/Fe junctions. If we follow the *ab initio* analysis of tunnelling in epitaxial MTJs [10, 11], we see that the conductivity related to the propagation of the interfacial resonance manifests as sharp peaks located at specific values of $k_{\|}$. Interestingly, these peaks do not correspond, as typically expected within the free-electron model for electrons, to a k normal to the insulating layer ($k_{\|} = 0$). Moreover, one can roughly associate the peaks in the conductivity with the minority spin surface state of Fe(001). This is represented in the sketched diagram of the minority surface band structure of Fe(001) shown in figure 4. At the Fermi level, the surface state crosses E_F for a specific value $k_{\|} \neq 0$. Moreover, the contribution to the conduction of the surface state becomes significant when it lies within a bulk band (dark areas in the E–k diagram), a situation when the surface state becomes an interfacial resonance state (IRS).

In the small MgO thickness regime, the carbon impurities at the Fe/MgO interface play no significant role in the tunnelling. From magnetization curve measurements, describing the equilibrium (zero-bias) transport properties, no significant effect of the C on the antiferromagnetic interactions has been observed (similar behaviour of samples of types A and B). If we consider the complex tunnelling landscape in this regime, one can see that the C–Fe bonding does not affect the d_{z^2}-like resonance state of Fe, whose propagation dominates the equilibrium tunnelling currents.

The physics of the equilibrium tunnelling presented above seems complex, due to the implication in the coupling of Bloch states with different symmetries, and also of the interfacial resonance of Fe. Moreover, in the low thickness regime one has to take into account the significant contribution to the tunnelling of electrons with $k_{\|} \neq 0$. These aspects would

require a multi-channel tunnelling model, each tunnelling channel being associated with a specific symmetry or resonance state. However, a 'conciliation' with the simplified mono-channel model of Slonczewski could be made, if one considers that the parameters used within this model are effective, and includes the complex aspects of the multi-channel tunnelling landscape, mentioned above.

3.2. Non-equilibrium tunnel transport regime

The tunnelling 'landscape' becomes different in the asymptotic regime, at large MgO thickness, where the symmetry-dependent rate decay in the barrier will reduce the number of propagating Bloch states. Moreover, the propagation of the interfacial resonance is strongly attenuated, having in view its rapid decay in the barrier. The filtering effect in k of the MgO barrier [10] determines a strong reduction of conductivity for electrons with $k_{\|} \neq 0$ when the thickness of MgO increases. This is assisted by the vanishing of the equilibrium tunnelling via the interfacial resonances, located at E_{F} for significantly large $k_{\|} \neq 0$, as shown in figure 4. However, if we follow figure 4, we see that the surface state of Fe may be 're-activated' by biasing the junction. Then, the electrons arrive with an energy $E = E_{\mathrm{F}} + eV$. Above E_{F}, the surface state crosses the bulk bands and becomes an interfacial resonance coming towards $\bar{\Gamma}$, which corresponds to propagating electrons with ($k_{\|} = 0$).

However, we should mention that for large thickness the structural quality of the MgO layer is slightly reduced. Indeed, after a pseudomorphical growth of MgO on Fe up to about five monolayers, a plastic relaxation occurs. This will induce dislocations within the barrier. These dislocations can behave as local 'defects', where the symmetry is broken and the conservation of $k_{\|}$ is destroyed. Therefore, they induce additional scattering with detrimental re-mixing effects in the symmetry filtering. This complicates the theoretical framework of analysis, valid for perfect mono-crystalline stacks where $k_{\|}$ is fully conserved.

The analysis of the large MgO thickness regime is performed using magneto-transport measurements (non-equilibrium transport) on patterned tunnel junctions, with lateral size between 50 and 200 μm.

3.2.1. MTJs with clean Fe/MgO interfaces. Lets us first consider the TMR(V) characteristics illustrated in figure 5(a), measured on sample B with carbon free Fe/MgO interface. As predicted theoretically [10, 11], for large MgO thickness in the asymptotic regime, the tunnelling is found to be dominated by a majority spd-like character state Δ_1 in the parallel (P) configuration. The propagation of this state in the antiparallel (AP) configuration should be prohibited, which corresponds to a strongly reduced conductivity. Within this framework, we measure a large TMR signal (inset of figure 5(a)), above 150% at room temperature. The slightly asymmetric bias-dependence can be explained by slightly asymmetric top and bottom Fe/MgO interfaces in terms of roughness, structural defects (dislocations) and the lattice distortions. The limited maximum value of the TMR with respect to theoretical predictions implicates a loss in the filtering efficiency, due to the structural imperfections enumerated above, over our large area junctions. We mention that all the junctions subjected to our study have a lateral size larger than 50 μm, which is several hundreds of times larger than the submicronic junctions in which higher TMR effects have been reported [7, 8].

Moreover, the TMR shows a significant variation with the applied voltage, especially in the small voltage range. From the conductivity in the P and AP configurations (depicted in figure 5(b)), one can point out two distinct contributions to the TMR decrease in small voltage.

Firstly, from the inset of figure 5(b) within the 0–0.5 V bias range, one can observe the strong increase of the AP conductivity with the voltage (more than 50% of AP conductivity

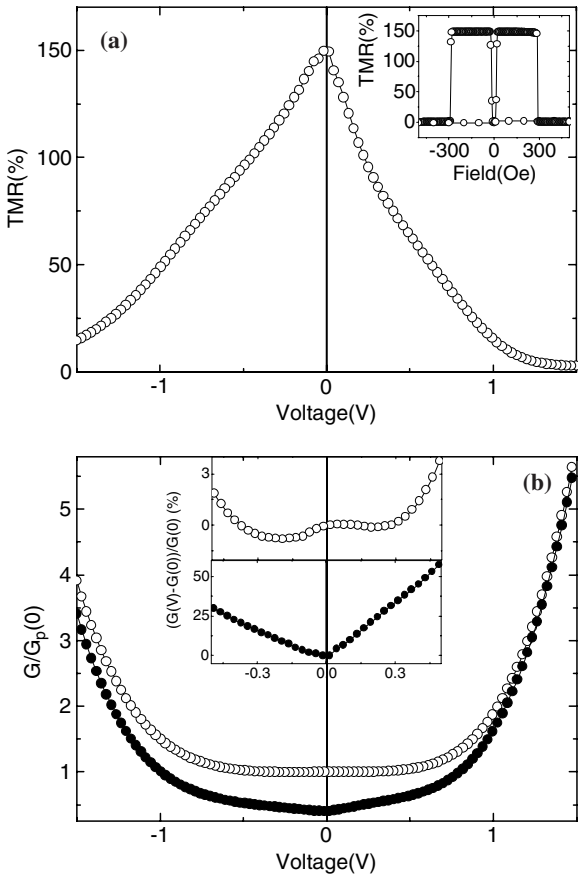

Figure 5. Magneto-transport characteristics for sample type B. In positive bias, the current flows from the top to the bottom electrode of the MTJ. (a) Bias variation of the TMR. Inset: typical TMR versus field loop measured at 10 mV. (b) Conductivity versus voltage curve, in the parallel (-o-) respectively anti-parallel (-●-) configuration of magnetization. Inset: relative variation of conductivity in the P and AP configurations in the small voltage regime.

variation, for less than 4% of variation for the P conductivity). We explain this enhancement of conductivity by evoking the contribution of the minority-spin interfacial resonance state of Fe to the tunnelling. This aspect is analysed in detail in the next paragraph.

Secondly, the conductivity in the parallel configuration presents a local minimum around 0.2 eV, in both positive and negative voltage. We quantify a conductivity variation of less than 1% between 0 V and the local minimum. The conductivity minimum reflects the dispersion of the energy bands of Fe(001); see figure 1. The top of the Δ_5 band lies at 0.2 eV above the Fermi level. When the energy of the hot electrons arriving across the barrier overcomes the top of this Δ_5 band, the conduction channel associated with this symmetry disappears. Therefore, the minimum of the P conductivity validates a Δ_5 contribution to the tunnelling at small bias (imperfect filtering). The amplitude of the relative variation of the conductivity from zero bias to the local minimum quantifies the zero-bias contribution of the Δ_5 electrons in the P channel conductivity, superposed on the corresponding Δ_1 one.

In conclusion, the two main factors responsible for the small bias TMR(V) both have an electronic structure origin: the contribution of the Δ_5 associated conduction channel in the

P configuration (imperfect filtering) and the contribution of the minority-spin IRS in the AP configuration. These represent common features for samples of types A and B. However, the magnitude of the related effects on the TMR is strongly dependent on the interfacial structure. Indeed, the chemical bonding at the interface in tunnel junctions plays a crucial role in the selection of tunnelling electrons [21].

3.2.2. MTJ with carbon contaminated bottom interface. The TMR(V) characteristic measured on sample A, with carbon impurities at the bottom Fe/MgO interface, appears strongly asymmetric with a maximum of TMR of 126% at room temperature (see figure 6(a)). This asymmetry reflects a net signature of the bcc Fe(001) electronic structure (mainly the d-like density of states features), and the contribution to the tunnelling of the interfacial resonance of Fe. Indeed, we have already shown the impact of interfacial resonance on the tunnelling [22] in MTJ systems with smaller MgO thickness. Here, for a 3 nm thick MgO barrier, having in view the rapid decay of the surface resonance in the barrier [14], the conductivity associated with this interfacial resonance should be overwhelmed by the dominance of the Δ_1 conduction channel. In our systems, this is what roughly happens in sample type B, with clean Fe/MgO interfaces.

However, when carbon impurities are inserted at the Fe/MgO bottom interface, the bonding between C and Fe (mainly via s, p-like orbitals) will drastically affect the propagation of the Δ_1 symmetry, without affecting the interfacial resonance of Fe, located in a d-like orbital. Preliminary *ab initio* calculations[3] [23] of Fe-C/MgO electronic structure show that the main effect of C on the surface state of Fe is a slight shift upwards in energy, with respect to the carbon free interface (figure 7). Similar effects, concerning the localization of Δ_1 electrons in the interfacial bonding, have been reported by Butler *et al* for oxygen impurities located at the interface Fe/MgO [25]. Moreover, as long as the associated-conductivity of the sp-like character state Δ_1 channel is reduced, one can expect an enhancement of the relative contribution to the tunnelling of the d-like states of the bcc Fe(001) (within $\Delta_{1,5}$ symmetries). Therefore, the TMR(V) will reflect the spectroscopy of the density of d-like states of the bcc Fe(001).

For positive biasing of the bottom electrode, the electrons, extracted from the top Fe(001) electrode by tunnelling across the barrier, 'scan' in energy the bottom 'flat' Fe(001) electronic structure. Then, when the energy of the collected electrons 'matches' the energy of the interface resonant state, a strong enhancement of the antiparallel conductivity with respect to the parallel one occurs, via the enhancement of the wavefunction matching at the interface. This is directly reflected by the sign reversal of the TMR (figure 6(a)) and by the antiparallel conductance which overcomes the parallel one, above 0.2 eV.

Here again, the P conductivity presents a minimum, when the energy of the hot electrons overcomes the one of the Δ_5 band. The inset of figure 6(b) illustrates a variation of the P conductivity of more than 2% between zero and the local minimum. Compared with the variation observed in samples of type B with clean interfaces, one can observe that here the contribution of the Δ_5 electrons to the tunnelling is more important. This 'loss' in the filtering efficiency is directly reflected by the amplitude of the TMR effect which is reduced in samples A with carbon contaminated bottom interfaces. Moreover, here the structural quality of the top MgO/Fe interface is reduced with respect to the atomically flat bottom one. Indeed, the bottom Fe was annealed at 450 °C whereas the top Fe electrode in junctions of type A was not. The

[3] We calculated the electronic structure of the Fe/Fe-C/MgO/Fe stack using the full potential–linear augmented plane wave (FP-LAPW) Wien2k code [24]. In our calculation, we used a supercell consisting of ten Fe layers, sandwiched in between six MgO layers. In order to describe the Fe-C/MgO interface a monolayer of C has been alternatively considered at 0.4 Å above the interfacial Fe.

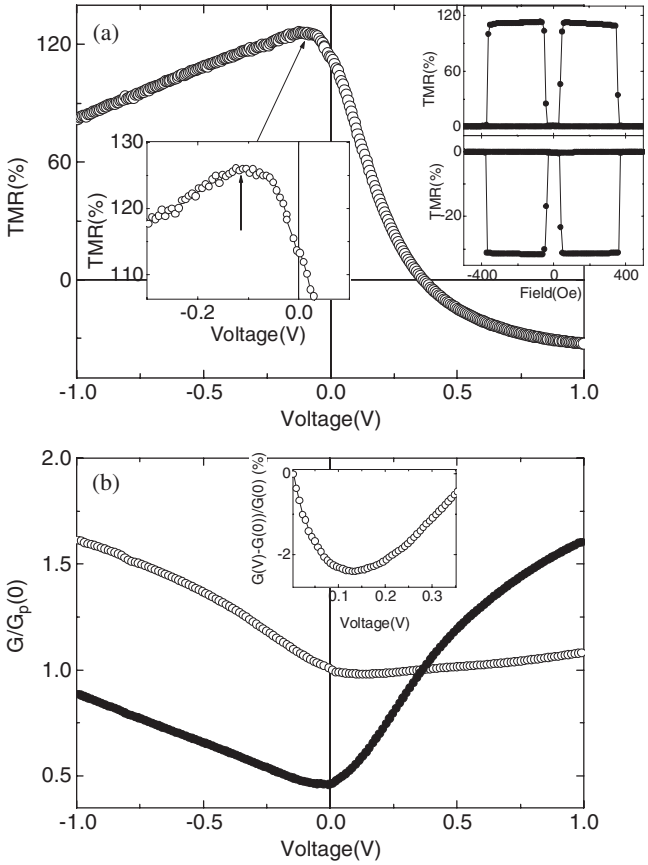

Figure 6. Magneto-transport characteristics TMR versus voltage for sample type A. In positive bias, the current flows from the top to the bottom electrode of the MTJ. (a) Bias variation of the TMR. Right inset: typical positive TMR–H loop measured at -10 mV, and negative TMR–H curve measured at $+0.6$ V, after the TMR reversal. Left inset: zoom around the maximum of the TMR. (b) Conductivity versus voltage curve, in the parallel (-o-) respectively anti-parallel (-•-) configuration of magnetization. Top inset: relative variation of parallel conductivity in the small positive voltage regime, around the local minima.

RHEED patterns and also the atomic force microscopy experiments validate a significantly higher roughness of the top Fe electrode in sample type A. One can assume that for this electrode the interfacial resonance is destroyed by roughness (localized minority surface state of top Fe not coupled to the bulk), and also that the density of states of the rough electrode presents no sharp features. Then, for negative voltage, when the electrons tunnel towards the positively biased rough top electrode, we observe a very small variation of the magnetoresistance versus V ($V_{1/2} > 1.5$ V) (also illustrated by $\mathrm{dTMR}/\mathrm{d}V$; see figure 8(b)). Moreover, the maximum of the TMR is not centred in zero bias, which implicates an increase of the TMR with the voltage (left inset in figure 6(a)). The increase of the TMR with the applied bias has already been theoretically predicted by Zhang *et al* [26]. The increase originates from an increase of the tunnelling polarization/filtering efficiency of the emitter negatively biased bottom electrode due to the contribution to the tunnelling of the electrons located below the Fermi level within an energy range $[E_F\text{–eV}, E_F]$. This contribution is dominated by the decrease of the minority IRS contribution to the conductivity (non-negligible at zero bias) and activation of the contribution

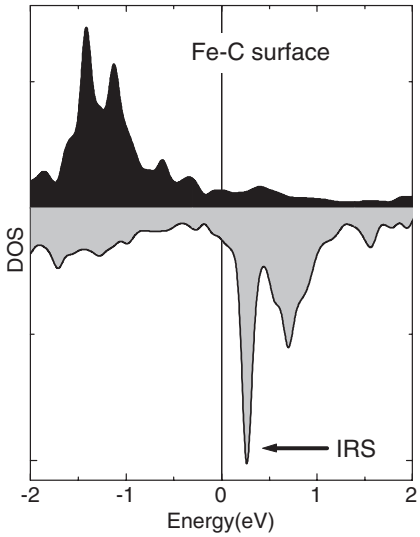

Figure 7. Surface density of state for majority (black) and minority (grey) spins, in an energy range ±2 eV around the Fermi level, for the interfacial Fe contaminated by C impurities, in an Fe/Fe-C/MgO stack. The calculation was performed using the full potential linear augmented plane wave method [24]. One can note the minority IRS of Fe at ∼0.3 eV above E_F.

of majority IRS located below E_F. Moreover, the extremely small decay of the TMR with the applied voltage indicates that an electronic-structure voltage variation mechanism related to the bottom Fe electronic structure competes with all the mechanisms responsible for the zero-bias anomaly, observed in sample type B, where a significant decay of the TMR with bias has been measured.

A more detailed analysis, in terms of tunnelling spectroscopy, for the voltage variation of the TMR is provided in the next paragraph.

3.2.3. Tunnelling spectroscopy analysis. Several mechanisms may explain the voltage variation of the tunnel magnetoresistance. These mechanisms are (i) incoherent tunnelling due to scattering at impurities or defects located in the barrier [27]; (ii) quenching of TMR by hot electrons or spin excitation of magnons [29]; (iii) energy dependence of spin-polarized DOS, which affects the spin polarization [28]. In our single-crystalline MTJ, the first mechanism should be less important than in a standard MTJ with poly-crystalline electrodes and amorphous barriers. In single-crystal junctions, the quality of the insulation is rigorously controlled by the 2D epitaxial growth. However, the dislocations within the insulating barrier and at the interfaces will induce imperfect filtering effects and will complicate the analysis of tunnelling in terms of symmetry/orbital character related channels. Concerning the second mechanism, the analysis of the magnon spectra for the bcc Fe [30], and phonon spectra for MgO [31], shows no relevant peak in the magnon/phonon DOS in the energy range where we analyse the voltage variation of the TMR. Therefore, we relate the observed TMR(V) in our junctions to the third mechanism, which points out the signature of the electronic structure in the tunnel transport characteristics. This signature is different for samples of type A and B which, despite a similar bottom Fe electrode, have different bottom interface and top electrode structural quality. In sample type B, the tunnelling of Δ_1 electrons is dominant, with a smaller Δ_5 contribution due to the imperfect filtering, as illustrated before. The contribution of the d-DOS features to the

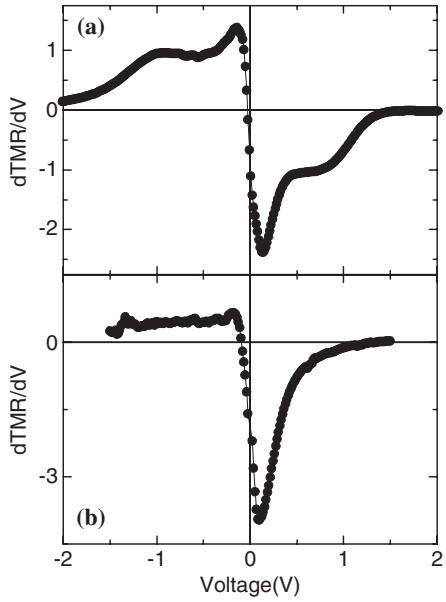

Figure 8. First derivative of the TMR versus voltage for (a) sample type B with clean Fe/MgO interfaces and (b) sample type A with carbon interfacial impurities.

TMR(V) is expected to be negligible. In samples of type A, the structural quality of the top Fe electrode is reduced (top Fe not annealed). One can assume that the energy dependence of spin-polarized DOS of this electrode, above the Fermi level, is small (no sharp features). Therefore the electronic structure contribution to the TMR(V) will reflect the electronic structure below E_F of the bottom flat Fe electrode, mainly the d-like character, having in view the selection at the bottom Fe-C/MgO interface previously discussed.

(a) MTJ with clean Fe/MgO interfaces. In samples of type B, the derivative of the TMR as a function of the voltage (shown in figure 8(a)) presents net peaks in both positive and negative voltages. These peaks are similar to those observed in standard junctions corresponding to inelastic excitation energy [20]. One can remark an almost symmetric behaviour, as expected for the quasi-symmetric structural quality of top and bottom electrodes. The signature of tunnelling transport is more clearly illustrated by the second derivative of the current, as shown in figure 9. In figure 9(a) we present the d^2I/dV^2 curves for samples of type B, with clean Fe/MgO interfaces. The AP conductivity is small, being dominated by the Δ_5 channel with a d-like orbital character. Indeed, in the AP configuration, an injected Δ_1 state cannot find equivalent symmetry in the second electrode. On the other hand, any spin-flip mechanism would drive a majority Δ_1 state into a minority Δ_1 state in the second electrode and would increase drastically the conductivity. However, if we analyse the magnon DOS spectra of the bcc Fe [30] we do not expect any magnon related peak of conductivity in the energy range where we observe the peak in the second derivative of the current. On the other hand, if we take into account the IRS located in the minority band, with a d_{z^2} orbital character belonging to the Δ_1 symmetry, one can expect a resonant tunnelling event when this IRS is activated. This would explain an enhancement of the AP conductivity via a resonant assisted mechanism, directly related to the interfacial resonance of the Fe(001). In the P configuration; the conduction is dominated by a majority channel associated with the Δ_1 state, with a mostly s-like orbital

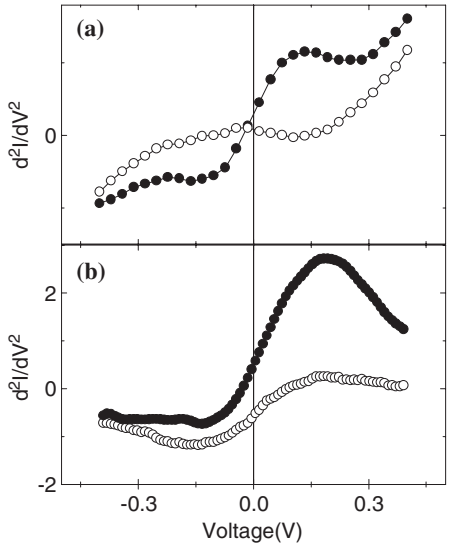

Figure 9. $\mathrm{d}^2I/\mathrm{d}V^2$ spectra, at low voltage, corresponding to P configuration (-o-) and AP configuration (-•-). (a) Sample type B, with clean interfaces. One can remark positive peaks only in the AP configuration. (b) Sample type A with carbon contaminated bottom interface. One can remark positive peaks in both P and AP configurations.

character, having in view the filtering in the MgO thick barrier. However, one can observe the local minima of the conductivity, around 0.2 eV, which point out the Δ_5 contribution to the tunnelling. There is no contribution of the IRS to the P conductivity. Therefore, from the $\mathrm{d}^2I/\mathrm{d}V^2$ spectra shown in figure 9(a) one can remark the net signature of resonant tunnelling only in the AP configuration. Corresponding to the P configuration, one can only observe the local minima of the conductivity, around 0.2 eV, when the zero-bias Δ_5 contribution disappears.

(b) MTJ with carbon contaminated bottom interface. A completely different voltage behaviour of junctions of type A shows the major importance of carbon impurities at the bottom interface. As illustrated in figure 8(b), the TMR derivative shows strongly asymmetric features, as expected for strongly asymmetric top/bottom electrodes. The strong dip in the derivative in the positive bias corresponds to the activation of the resonant assisted tunnel mechanism by the minority IRS in AP configuration, around 0.2 eV when it gets in $k_{\|} = 0$ (as shown in the sketch of figure 4). The contribution of the IRS to the tunnelling is strongly enhanced by the carbon presence at the bottom interface which drives the conductivity sensitive to d-like electrons, whose orbital character the IRS belongs to. On the other hand, in negative voltage one can only remark a faint 'echo' of the corresponding peak observed in samples B (figure 8(a)). Here one can assume that the roughness destroys the IRS at the top MgO/Fe interface.

The second derivative of the current (figure 9(b)) illustrates here resonant tunnelling events in both AP and P configurations, dominated by the peak in the positive voltage for the AP configuration, related to the IRS-related reversal of the TMR. To our knowledge, no theoretical investigation of tunnelling properties in carbon contaminated Fe/MgO MTJ has been performed up to now. Based on preliminary theoretical investigation [23] (see footnote 3), we propose here a possible interpretation of our experimental results. The role of the interfacial carbon impurities is to select the tunnelling electrons in terms of their orbital character. By reducing the associated conductivity of the s-like component of the Δ_1 electrons, in carbon contaminated

junctions the tunnel transport gets more sensitive to the d-like features, which otherwise were attenuated at large MgO thickness. Moreover, the carbon breaks the cubic symmetry at the interface, which will induce a 'remixing' effect in term of symmetry between the d components of the Δ_1 and Δ_5 states. First, this would implicate a much stronger influence of the interfacial resonance state with a d_{z^2} character in the conductivity. In the AP configuration, the resonant enhancement of the conductivity occurs when the d_{z^2} component of the injected Δ_1 symmetry finds an equivalent symmetry state in the IRS on the other electrode. The AP conductivity overcomes the parallel one, reversing the sign of the tunnel magnetoresistance. Second, the reduction of filtering efficiency reflected by the enhancement of the relative contribution of the Δ_5 channel in samples with C at the interface is illustrated by the second derivative of the current in the parallel configuration. In figure 9(b) one can observe the presence of peaks in d^2I/dV^2 corresponding to P configuration in both positive and negative voltages. Indeed, these peaks are related to the Δ_5 conduction channel which 'vanishes' at 0.2 eV when the energy of the tunnelling electrons overcomes the top of the Δ_5 band (see figure 1).

In our explanation for the zero-bias anomaly observed in epitaxial Fe/MgO/Fe junctions we excluded the implication of magnons. This was done only based on theoretical calculations for magnon spectra, which show no peak in the magnon DOS in the relevant energy range. However, a complete proof for a dominant interfacial electronic structure origin of the zero-bias anomaly should be provided by further experiments concerning transport properties at low temperature, below the freezing temperatures of magnons in Fe. Moreover, our experimental results motivate further theoretical investigations which should confirm or invalidate the resonant transport mechanisms we propose here.

4. Conclusion

Spin-polarized transport properties in epitaxial Fe(100)/MgO/Fe tunnel junction stacks have been investigated in two 'extreme' regimes. First, for very thin MgO layers, we show that the equilibrium tunnel transport between the two Fe electrodes across the barrier induces an interesting antiferromagnetic interaction. This antiferromagnetic coupling effect is explained in terms of spin-polarized tunnelling. If we take into account the specific aspects of the electronic transport in mono-crystalline multilayers, one has to consider a complex, symmetry-related multi-channel model for the tunnelling with a dominant contribution of the Fe(001) minority resonance state, whose dominant tunnelling determines the sign of the coupling. Second, for large MgO thickness in the asymptotic regime, we observed as predicted theoretically large magnetoresistive effects, directly related to the band structure characteristics of the Fe/MgO/Fe junctions. Moreover, we illustrate that the interface chemical structure plays a crucial role in the filtering of tunnelling electrons in terms of symmetry and orbital character. Our results show that the interface engineering in Fe/MgO/Fe MTJs represents a strong tool to control the magneto-transport properties of spintronic devices. Therefore, the magneto-transport properties of epitaxial tunnel junctions may be skilfully engineered to achieve new functionality when the tunnel junction is used as an elementary brick in any spintronic device.

Acknowledgments

CT acknowledges D Stoeffler for fruitful discussions concerning the electronic structure and its implication in tunnelling, E Snoeck for transmission electron microscopy analysis of our samples and D Ligiardi and M Alnot for technical support.

References

[1] Moodera J S, Kinder L R, Wong T M and Meservey R 1995 *Phys. Rev. Lett.* **74** 3273
[2] Wolf S A 2000 *J. Supercond.* **13** 195
Daughton J M 1997 *J. Appl. Phys.* **81** 3758
Gallagher W J, Kaufman J H, Parkin S S P and Scheuerlin R E 1997 *US Patent Specifiation* 5 640 343
[3] Bowen M, Cros V, Petroff F, Fert A, Martinez Boubeta C, Costa-Kramer J L, Anguita J V, Cebollada A, Briones F, de Teresa J M, Morellon L, Ibarra M R, Guell F, Peiro F and Cornet A 2001 *Appl. Phys. Lett.* **79** 1655
[4] Faure-Vincent J, Tiusan C, Jouguelet E, Canet F, Sajieddine M, Bellouard C, Popova E, Hehn M, Montaigne F and Schuhl A 2003 *Appl. Phys. Lett.* **82** 4507
[5] Yuasa S, Fukushima A, Nagahama T, Ando K and Suzuki Y 2004 *Japan. J. Appl. Phys.* B **43** (4)
[6] Yuasa S, Nagahama T, Fukushima A, Suzuki Y and Ando K 2004 *Nat. Mater.* **3** 868
[7] Parkin S S P, Kaiser C, Panchula A, Rice P M, Hughes B, Samant M and Yang S-H 2004 *Nat. Mater.* **3** 862
[8] Djayaprawira D D, Tsunekawa K, Nagai M, Maehara H, Yamagata S, Watanabe N, Yuasa S, Suzuki Y and Ando K 2005 *Appl. Phys. Lett.* **86** 092502
[9] Tiusan C *et al* 2006 to be published
[10] MacLaren J M, Zhang X-G, Butler W H and Wang X 1999 *Phys. Rev.* B **59** 5470
Butler W H, Zhang X-G, Schulthess T C and MacLaren J M 2001 *Phys. Rev.* B **63** 054416
[11] Mathon J and Umerski A 2001 *Phys. Rev.* B **63** 220403(R)
[12] Stroscio J A, Pierce D T, Davies A, Celotta R J and Weinert M 1995 *Phys. Rev. Lett.* **75** (16) 2960–3
[13] Wunnicke O, Papanikolaou N, Zeller R, Dederichs P H, Drchal V and Kudrnovsky J 2002 *Phys. Rev.* B **65** 064425
[14] Ding H F, Wulfhekel W, Henk J, Bruno P and Kirschner J 2003 *Phys. Rev. Lett.* **90** 116603
[15] Slonczewski J C 1989 *Phys. Rev.* B **39** 6995
[16] Faure-Vincent J, Tiusan C, Bellouard C, Popova E, Hehn M, Montaigne F and Schuhl A 2002 *Phys. Rev. Lett.* **89** 107206
[17] Zhuravlev M Y, Tsymbal E Y and Vedyayev A V 2005 *Phys. Rev. Lett.* **94** 026806
[18] Blum V, Schmidt A, Meier W, Hammer L and Heinz K 2003 *J. Phys.: Condens. Matter* **15** 3517
[19] Popova E, Faure-Vincent J, Tiusan C, Bellouard C, Fischer H, Hehn M, Montaigne F, Alnot M, Andrieu S, Schuhl A, Snoeck E and da Costa V 2002 *Appl. Phys. Lett.* **81** 1035
[20] Moodera J S, Nowak J and vandeVeerdonk R J M 1998 *Phys. Rev. Lett.* **80** 2941
[21] Zhang X-G and Butler W 2003 *J. Phys.: Condens. Matter* **15** R1603
[22] Tiusan C, Faure-Vincent J, Bellouard C, Hehn M, Jouguelet E and Schuhl A 2004 *Phys. Rev. Lett.* **93** 106602
[23] Stoeffler D 2005 private communication
[24] Blaha P, Schwarz K, Madsen G K H, Kvasnicka D and Luitz J 2001 WIEN2k *An Augmented Plane Wave + Local Orbitals Program for Calculating Crystal Properties* ed K Schwartz (Austria: Techn. Univ. Wien) ISBN 3-9501031-1-2
[25] Zhang X-G, Butler W H and Bandyopadhyay A 2003 *Phys. Rev.* B **68** 092402
[26] Zhang C, Zhang X-G, Krstic P S, Cheng H-P, Butler W H and MacLaren J M 2004 *Phys. Rev.* B **69** 134406
[27] Jansen R and Moodera J S 2000 *Phys. Rev.* B **61** 9047
[28] de Teresa J M, Barthelemy A, Fert A, Contour J P, Montaigne F and Seneor P 1999 *Science* **286** 507
[29] Zhang S, Levy P M, Marley A C and Parkin S S P 1997 *Phys. Rev. Lett.* **79** 3744
Moodera J S, Nowak J and van de Veerdonk R J M 1998 *Phys. Rev. Lett.* **80** 2941
[30] Pajda M, Kudrnovsky J, Turek I, Drchal V and Bruno P 2001 *Phys. Rev.* B **64** 174402
[31] Parlinski K, Lazewski J and Kawazoe Y 2000 *J. Phys. Chem. Solids* **61** 87